JOURNAL OF PROPULSION AND POWER
Vol. 21, No. 6, November–December 2005

Mach Number and Freestream Turbulence Effects on Turbine Vane Aerodynamic Losses

Qiang Zhang,* Donald Sandberg,† and Phillip M. Ligrani‡
University of Utah, Salt Lake City, Utah 84112-9208

The aerodynamic performance of a smooth, cambered turbine vane (which replicates one used in an operating gas turbine engine) is investigated in this paper. Three different Mach-number distributions are employed, which result in one transonic flow and two subsonic flows. All of these distributions match flow conditions in different industrial applications. A fine mesh grid and cross bars are used to augment the magnitudes of longitudinal turbulence intensity at the inlet of the test section. Wake-profile data are presented for two different locations downstream of the vane trailing edge (one axial chord length and 0.25 axial chord length). The contributions of varying Mach number and varying freestream turbulence intensity to aerodynamic losses, normalized kinetic energy profiles, normalized Mach-number profiles, integrated aerodynamics losses, and area-averaged loss coefficients are quantified. Results show that wake profiles are more sensitive to turbulence intensity variations at lower subsonic flow conditions than when transonic flow is present. Wake profiles are also broadened either as the exit Mach number increases or as the freestream turbulence intensity level increases. Higher losses in the freestream flow are present as the inlet turbulence intensity level increases. Also described are effects of increased turbulent diffusion, streamwise development, and profile asymmetry. Corresponding integrated aerodynamic losses and area-averaged loss coefficient Y_A magnitudes increase with increasing Mach number or with increasing turbulence intensity level. Results additionally show larger loss magnitudes with flow turning and cambered airfoils, relative to symmetric airfoils, when compared at the same exit Mach number.

Nomenclature

Bx	=	linear distance measured along the axial chord from vane leading edge
C_p	=	local total pressure coefficient, $(P_{oi} - P_{oe})/P_{oi}$
c	=	true chord length
c_x	=	axial chord length
M_e	=	exit local Mach number
M_{ex}	=	exit freestream Mach number measured 0.25 axial chord lengths downstream of the vane trailing edge
$M_{e,\infty}$	=	exit freestream Mach number
KE	=	normalized local kinetic energy, $(P_{oe} - P_{se})/(P_{oe} - P_{se})_\infty$
k	=	roughness height
p	=	passage pitch
P_o	=	stagnation pressure
P_{oe}	=	exit local stagnation pressure
$P_{oe,m}$	=	mass-averaged exit stagnation pressure
$P_{oe,\infty}$	=	exit freestream stagnation pressure
P_{oi}	=	inlet stagnation pressure
P_{se}	=	exit local static pressure
$p_{oe,A}$	=	area-averaged exit total pressure
$p_{se,A}$	=	area-averaged static pressure
$q_{e,m}$	=	exit mass-weighted dynamic pressure
Re	=	Reynolds number based on true chord length
Tu	=	test-section inlet longitudinal turbulence intensity level
u	=	exit local streamwise velocity
x	=	streamwise coordinate at the exit of the test section
Y_A	=	area-averaged loss coefficient
y	=	normal coordinate at the exit of the test section
ρ	=	exit local density
ω	=	total pressure loss coefficient used by Ames and Plesniak,[4] $(P_{oi} - P_{oe})/(P_{oi} - P_{se})$

Subscripts

A	=	area averaged
e	=	exit
∞	=	freestream

Introduction

INTEREST in the effects of the freestream turbulence levels and Mach numbers on the aerodynamic performance of turbine vanes and blades is increasing. Of the investigations that examine the effects of augmented freestream turbulence levels, Gregory-Smith and Cleak[1] show that the mean flowfield is not affected significantly by inlet turbulence intensity levels as high as 5%. Variations of the different Reynolds-stress tensor components and spectra are given for different cascade locations, which show important changes near the endwall as mainstream turbulence levels are augmented. Giel et al.[2] employ an active blowing grid of square bars to produce a turbulent intensity and length scale of 10% and 22 mm, respectively, at the entrance of a transonic cascade. Heat-transfer results are given along a turbine airfoil, which show the effects of strong secondary flows, laminar-to-turbulent transition, and variations near the stagnation line. Boyle et al.[3] provide turbine vane aerodynamic data at low Reynolds numbers made at midspan locations downstream of a linear cascade with inlet turbulence intensity levels as high as 10%. In a study of aerodynamic losses downstream of subsonic turbine airfoil with no film cooling, Ames and Plesniak[4] demonstrate important connections between wake growth and the level of freestream turbulence. Wake mixing and eddy diffusivity magnitudes, in particular, are altered by different levels of freestream turbulence. Jouini et al.[5] present detailed measurements of midspan aerodynamics performance characteristics of a transonic turbine cascade at off-design conditions. Measurements of blade loading, exit flow angles, and trailing-edge base pressures at different Mach numbers show that profile losses at transonic conditions are closely related to base

Received 28 November 2004; revision received 15 March 2005; accepted for publication 31 March 2005.

*Graduate Student, Convective Heat Transfer Laboratory, Department of Mechanical Engineering.
†Graduate Student, Convective Heat Transfer Laboratory, Department of Mechanical Engineering.
‡Professor, Convective Heat Transfer Laboratory, Department of Mechanical Engineering.

pressure behavior. Radomsky and Thole[6] present measurements of time-averaged velocity components and Reynolds stresses along a turbine stator vane at elevated freestream turbulence levels. As the freestream turbulence level increases, transition occurs farther upstream on the suction side, with increased velocity fluctuations near the pressure side. Boyle et al.[7] provide aerodynamic data for a linear turbine vane cascade, including surface-pressure distributions and aerodynamic losses for different Reynolds numbers, Mach numbers, and levels of inlet turbulence.

Investigations by Zhang et al.[8] and Zhang and Ligrani[9]employ symmetric airfoils with no camber and without significant flow turning. Of these, Zhang et al.[8] investigate the effects of surface roughness and turbulence intensity on the aerodynamic losses produced by the suction surface of a symmetric turbine airfoil. Their results show that the effects of different inlet turbulence intensity levels are generally relatively small, diffusion from the wake to surrounding freestream flow results in broader wakes with more uniform aerodynamic wake loss distributions. Without the presence of freestream losses, the magnitudes of integrated aerodynamic losses decrease slightly as the inlet turbulence intensity increases. Zhang and Ligrani[9] investigate the effects of surface roughness, freestream Mach number, and turbulence intensity on the aerodynamic performance of turbine airfoils. Their data show that increasing freestream Mach number produce larger magnitudes of nondimensional total pressure loss coefficients. Magnitudes of integrated aerodynamic losses change by a much larger amount as either the freestream Mach number or turbulence intensity are altered, when the airfoil is roughened (compared to smooth airfoil results).

Of the investigations that examine the effects of Mach number, Joe et al.[10] show that total pressure losses for a high-pressure turbine vane increase approximately with the square of the exit Mach number as a result of a decrease in boundary-layer thickness. Coton et al.[11] investigate the effects of Reynolds number and Mach number on the profile losses of a conventional low-pressure turbine rotor cascade and report that the exit Mach number affects the losses through a modification of the pressure gradient imposed on the boundary layer. Their investigations indicate that loss levels are fairly constant with the change of Mach number and are not sensitive to freestream turbulence level.

The present study is unique because new data are provided to clarify the separate and combined influences of Mach number and freestream turbulence level on aerodynamic performance of a cambered turbine vane. From analyses and comparisons of results from other recent investigations,[3,4,8,9] some of the inconsistencies from different investigations as a result of different experimental conditions and different methods to evaluate aerodynamic losses are addressed. The present investigation is different from the investigations of Zhang et al.[8] and Zhang and Ligrani[9] because the cambered turbine vane employed produces substantial flow turning and matches a vane configuration employed in a gas turbine application. Considered are the effects of freestream turbulence on aerodynamic losses downstream of the smooth vane for three different Mach-number distributions, which result in one transonic flow and two subsonic flows (and match flow conditions in three different industrial application environments). A mesh grid and cross bars are used to augment the magnitudes of longitudinal turbulence intensity at the inlet of the test section. Wake-profile data are presented for two different locations downstream the vane trailing edge, which illustrate the influences of varying freestream turbulence intensity level and vane Mach number on local aerodynamic losses, local Mach numbers, local kinetic energy, integrated aerodynamics losses (IAL), and area-averaged loss coefficient. As such, the present data provide useful information to designers of turbomachinery components and to individuals developing models for computational-fluid-dynamics predictions.

Experimental Apparatus and Procedures

Transonic Wind Tunnel

The University of Utah Transonic Wind Tunnel (TWT) is used for the study because it produces Mach numbers, pressure variations, Reynolds numbers, passage mass flow rates, and scaled physical dimensions, that match values along airfoils in operating aeroengines and in gas turbines used for utility power generation. The TWT blowdown-type facility consists of two main parts: 1) compressor and storage tanks and 2) wind tunnel. The wind tunnel consists of five major subsections: 1) flow rate and pressure level management apparatus; 2) plenum tank; 3) inlet ducting and test section; 4) plenum, exit ducting, and ejector; and 5) control panel. Detailed descriptions are provided by Zhang and Ligrani,[9] Jackson et al.,[12] and Furukawa and Ligrani.[13]

A Gardner Denver Company model RL-1155-CB compressor is used to pressurize the array of eight tanks whose total capacity volume is 11.9 m^3. A VanAir VAS93039 model D16-5 Deliquescent desiccant dryer, a Pall Corporation 5EHG-4882-207 oil filter, and two Permanent Filter Corporation No. 13846 particulate filters are located just downstream of the compressor to remove particulates and moisture from the air. A Fisher pressure regulator with a 6×4 EWT design sliding gate valve, a Fisher type 667 diaphragm actuator, a 3582 series valve positioner, and a Powers 535 1/4 DIN process controller are used to regulate the pressure in the test section as the storage tanks discharge. A plenum tank, a 30.48-cm inner diameter pipe, a circular-to-square transition duct, a nozzle, and the test section then follow. The test section is connected to a large 92.71 by 91.44 by 91.44 cm plenum with a square plastic flange at its outlet. The plenum diffuses high-speed air from the test-section exit into a reservoir of low velocity air. This plenum is then connected to two ducts, which are subsequently connected to the atmosphere.

Experimental parameters for the three different operating conditions employed in this study are tabulated in Table 1.

Test Section and Test Vane

The present test section is designed to match Reynolds numbers, Mach numbers, pressure gradients, passage mass flow rates, boundary-layer development, streamline curvature, airfoil camber, and physical dimensions of turbine vanes in operating industrial engines. A schematic diagram of the test section with the cambered vane is shown in Fig. 1. The inlet of the test section is 12.70 by 12.70 cm. The side and bottom walls of the test section are made of steel, and the top wall is made up of acrylic. As shown in Fig. 1, two zinc-selenide windows are also placed on both of the side walls, so that the entire airfoil surface is accessible to optical, surface-temperature measurement schemes such as infrared thermography.

Table 1 Experimental operating conditions

Exit Mach number M_{ex}	0.35	0.50	0.71
Exit Reynolds number[a]	0.5×10^6	0.7×10^6	0.95×10^6
Inlet Reynolds number[a]	0.2×10^6	0.3×10^6	0.4×10^6
Inlet Mach number	0.15	0.19	0.23
Inlet total pressure, kPa	94	98	106
Inlet relative humidity	15–20%	15–20%	15–20%

[a]Based on true chord length.

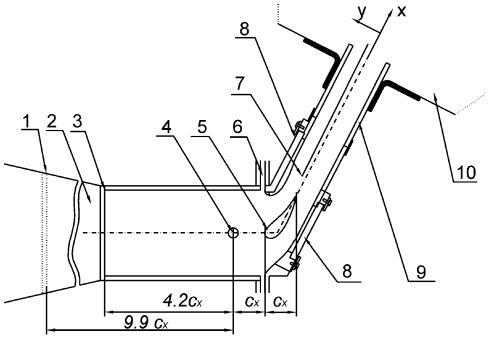

1. Bar Grid Position 2. Nozzle 3. Fine Mesh Grid Position
4. Inlet Pressure Probe and Thermocouple
5. Test Blade 6. Bleeding System
7. Exit Pressure Probe and Thermocouple
8. Zinc-Selenide Window 9. Tailboard 10. Exit Plenum

Fig. 1 Schematic diagram of the test section.

Table 2 Test vane geometric parameters

True chord c	7.27 cm
Axial chord c_x	4.85 cm
Pitch p	6.35 cm
Span	12.7 cm
Flow turning angle	62.75 deg

Appropriate cascade flow conditions are maintained, in part, by a pair of adjustable bleed ducts, which are located on the two side walls, as shown in Fig. 1. The flow rate of each bleed duct is regulated using an adjustable ball valve. Following these, the test-section walls have the same pressure-side and suction-side contours as the test vane. The exit area and exit flow direction from the cascade test section can be altered by changing the angles of the two exit tailboards, which are also shown in Fig. 1. Thus, 1) changing the total pressure at the test-section inlet using the pressure regulator/sliding gate valve arrangement, 2) changing the angular positions of the two tailboards, and 3) adjusting the ball valves of the bleeding system are employed to alter the Mach-number distribution along the vane in the test section, for a particular vane and test-section configuration. By adjusting these items, appropriate Mach-number distributions along the test vane are obtained, which are discussed later in the paper.

Table 2 gives geometric parameters of the test vane. The coordinates of this test vane profile were provided by personnel at Pratt and Whitney–Canada Corporation, along with the flow conditions present in the associated operating environment.

Pressure and Temperature Measurements

As tests are conducted, Validyne Model DP15-46 pressure transducers (with diaphragms rated at either 34.5 or 344.7 kPa) and calibrated copper-constantan thermocouples are used to sense pressures and temperatures at different locations throughout the facility. Signals from the pressure transducers are processed by Celesco Model CD10D carrier demodulators. All pressure transducer measurement circuits are calibrated using a Wallace and Tiernan FA145 bourdon tube pressure gauge as a standard. A United Sensor PLC-8-KL pitot-static probe with an attached, calibrated Watlow standard type-K copper-constantan thermocouple and a five-hole conical-tipped pressure probe (cone angle 15 deg) also with a similar Watlow thermocouple are used to sense total pressure, static pressure, and recovery temperature at the inlet and exit of the test section, respectively, during each blowdown. Mach numbers, sonic velocities, total temperatures, and static temperatures are determined from these data. The five-hole probe has a tip that is 1.27 mm in diameter and a stem that is 3.18 mm in diameter. Each port has a diameter of 0.25 mm. The overall response time of the pressure measuring system is about 0.2 s. The conical probe is aligned using two yaw ports placed on either side of the probe. The alignment using the two yaw ports is implemented at one location at the start of each traverse. The probe is located downstream of the vane such that the position in the streamwise direction is adjustable. As a blowdown is underway, it is traversed across a full pitch using a two-axis traversing sled with two Superior Electric M092-FF-206 synchronous stepper motors, connected to a Superior Electric Model SS2000I programmable motion controller and a Superior Electric Model SS2000D6 driver. Commands for the operation of the motion controller are provided by LABVIEW 7.0 software and pass though a serial port after they originate in a Dell Precision 530 PC workstation. Each profile is measured through the wake from minus y/Cx locations to positive y/Cx locations and then repeated as the probe is traversed in the opposite direction. The resulting data are subsequently averaged at each wake measurement location.

Voltages from the carrier demodulators and thermocouples are read sequentially using Hewlett-Packard HP44222T and HP44222A relay multiplexer card assemblies, installed in a Hewlett-Packard HP3497A low-speed data acquisition/control unit. This system provides thermocouple compensation electronically such that voltages for type-T thermocouples are given relative to 0°C. The voltage outputs from this unit are acquired by the Dell Precision 530 PC workstation through its USB port, using LABVIEW 7.0 software and a GPIB-USB-B adaptor made by National Instruments.

Augmenting Mainstream Flow Turbulence Levels

Three different arrangements are used at the inlet of the test section to produce three different levels of mainstream turbulence intensity: 1) no grid or bars, 2) fine-mesh grid, and 3) cross bars. The fine-mesh grid consists of an array of four square rods arranged horizontally and four square rods arranged vertically. Each rod is spaced 25.4 mm from adjacent rods and is 6.5 mm on each side. The open area amounts to 48% of the inlet area. The cross-bars device consists of two parallel bars, where each is 25.4 mm in width, with 25.4-mm spacing from the adjacent bar and 25.4-mm spacing from the top and bottom walls of the inlet duct. The open area amounts to 60% of the inlet area. Note that the installation positions for fine-mesh grid and bar grid are different because of consideration of inlet uniformity (see Fig. 1).

Longitudinal Turbulence Intensity Measurements

A single, horizontal-type platinum-plated tungsten hot-wire sensor, with a diameter of 12.7 μm and a length of 2.54 mm, is employed to measure the time-varying longitudinal component of velocity at the inlet of the test section. The time-averaged longitudinal velocity and the longitudinal turbulence intensity are then determined from these measurements. The measurement location is one axial chord length upstream of the vane leading edge. The hot-wire probe is driven by a Disa 55M10 constant-temperature hot-wire anemometer bridge with an overheat ratio of 1.6. The analog signal from this bridge is then processed using a Dantec 56N20 signal conditioner with a low-pass, antialiasing filter set to 100 kHz. The time-varying output voltage signal is then sampled at a 200-kHz rate using a DATEL PCI441D I/O board installed in the Dell Precision 530 PC workstation. During each measurement, 2,000,000 voltage values are sampled over a time period of 10 s. Data are acquired using LABVIEW 7.0 software and then processed further using MATLAB 6.1 software. The entire measurement system, including the hot-wire sensor, is calibrated in the freestream of the TWT. A Kiel-type pressure probe, wall static taps, and a copper-constantan thermocouple are used to measure and determine the total pressure, static pressure, recovery temperature, and velocity at the inlet of the test section as the calibration is conducted.

Experimental Uncertainties

Uncertainty estimates are based on 95% confidence levels and determined using procedures described by Kline and McClintock[14] and by Moffat.[15] Mach-number uncertainty is 0.002. Uncertainty of temperatures is 0.15°C. Pressure uncertainty is 0.25 kPa. Uncertainties of C_p, M_e/M_e, and KE are 0.0013 (0.07), 0.0023 (0.96), and 0.03 (0.90), respectively, where typical nominal values of these quantities are given in parenthesis. IAL uncertainty is 0.04 N/cm (0.800 N/cm). Magnitudes of IAL, determined from replicate runs, are always within IAL uncertainty ranges.

Experimental Results and Discussion

Test-Section Flow Characteristics and Mach-Number Distributions

During each blowdown test, the total pressure, Reynolds number, and turbulence level at the test-section inlet are maintained in a continuous and steady fashion for 45-s-long time intervals. (Detailed information is provided by Jackson.[16]) Such characteristics are not only because of the TWT design, but also the excellent performance characteristics of the TWT mainstream air pressure regulator and its controller. During each test, the inlet total pressure at the inlet of the test section P_{oi} (one axial chord length upstream of the vane leading edge) is maintained constant for each experimental condition examined at either 94, 98, or 106 kPa. Corresponding exit freestream Mach numbers, measured 0.25 axial chord lengths downstream of the airfoil trailing edge, are 0.35, 0.50, and 0.71, respectively, and chord Reynolds numbers (based on exit flow conditions) are 0.5×10^6, 0.7×10^6, and 0.95×10^6, respectively. Table 1 gives

Table 3 Turbulence intensity levels at the inlet of the test section

Exit Mach number M_{ex}	0.35	0.50	0.71
No grid	1.6%	1.2%	1.1%
Fine-mesh grid	5.7%	5.4%	5.4%
Bar grid	8.2%	7.7%	7.7%

Table 4 Length scales at the inlet of the test section

Exit Mach number M_{ex}	0.35	0.50	0.71
Fine-mesh grid	2.2 cm	2.1 cm	2.7 cm
Bar grid	4.6 cm	4.6 cm	4.7 cm

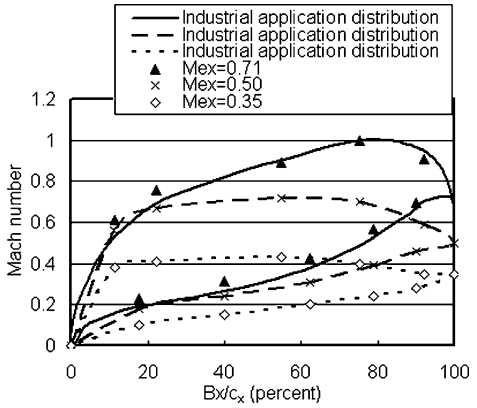

Fig. 2 Mach-number distributions along the test vane.

experimental conditions for the three different operating conditions, which are employed in this study.

Magnitudes of the inlet longitudinal turbulence intensity and length scale for the three exit Mach numbers are tabulated in Tables 3 and 4, respectively. Here, turbulence intensity is defined as the ratio of the rms of the longitudinal fluctuation velocity component divided by the local streamwise mean component of velocity. There are small differences of the turbulence intensity level for a same turbulence generator at three exit Mach numbers, as shown in Table 3. The turbulence level usually decreases as the velocity of the flowfield increases. The autocorrelation function is integrated with respect to the time lag to obtain the longitudinal integral timescale, which is then multiplied by the mean velocity to get the longitudinal integral length scale, which is a representative of the largest eddies in the turbulent flowfield.

Inlet uniformity measurements are conducted at five different pitchwise locations at the inlet of the test section. With no turbulence grid employed, the total pressure and static pressure show excellent spatial uniformity at this location, varying by less than 0.5% of mean values. With the fine-mesh grid and bar grid, the total pressure and static pressure generally vary less than 0.6% of mean values for all three operating conditions employed. Note that the bar grid is installed further away from the leading edge of the vane compared to the position of the fine mesh grid, as shown in Fig. 1. This maintains acceptable levels of uniformity in the flow as it approaches the vane.

Figure 2 shows the Mach-number distributions along the turbine vane pressure side and along the vane suction side for each of the three operating conditions. Each different operating condition is produced by setting a different stagnation pressure at the test-section inlet using the TWT mainstream air pressure regulator. Note that the exact same positions of the tailboards and the same flow settings on the bleeding system (shown in Fig. 1) are used for each flow condition. The data shown in Fig. 2 are based upon measurements of total pressure at the test-section inlet and vane midspan static pressures. Compressible flow analysis is used to calculate Mach-number distributions around the vane. These are measured using an airfoil that is constructed especially for this task. The vane has five pressure taps on the pressure side and five pressure taps on the suction side, as well as one pressure tap located on the leading edge at the vane midspan. As shown in Fig. 2, one Mach-number distribution employed in this study is transonic on the vane suction side and subsonic on the pressure side, and the other two operating conditions are completely subsonic. Note that a strong adverse pressure gradient is present on the suction side of the vane when $Bx/c_x > 0.80$ for $M_{ex} = 0.71$. Figure 2 also shows that the Mach-number distributions on pressure and suction sides for all three exit Mach numbers are in excellent agreement with data for gas turbine vanes from industry.

Local Aerodynamic Performance

Figures 3–8 present local aerodynamic performance data in the wake for the three mainstream Mach-number distributions and three freestream turbulence intensity levels. To provide an appropriate standard of comparison, each profile is measured over one complete exit pitch spacing (or one complete exit vane spacing). In addition, the inlet total pressure is always kept constant as different turbulence intensity levels are employed with the same mainstream Mach-number distribution.

The wake profiles shown in Figs. 3–8 are asymmetric. Suction-side wakes (at negative y/c_x) are thicker than the pressure side wakes (at positive y/c_x). The asymmetry in the wake is caused by loading on the vane surface and the past history of the flow. In

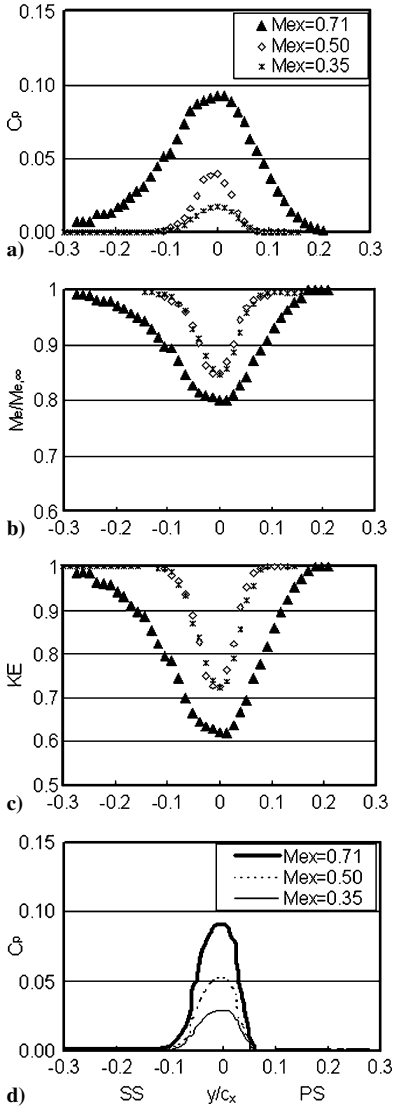

Fig. 3 Profiles measured at one axial chord length downstream of the test vane without turbulence generator installed: a) normalized local total pressure losses, b) normalized local Mach numbers, c) normalized local kinetic energy, and d) FLUENT predictions of C_p profiles.

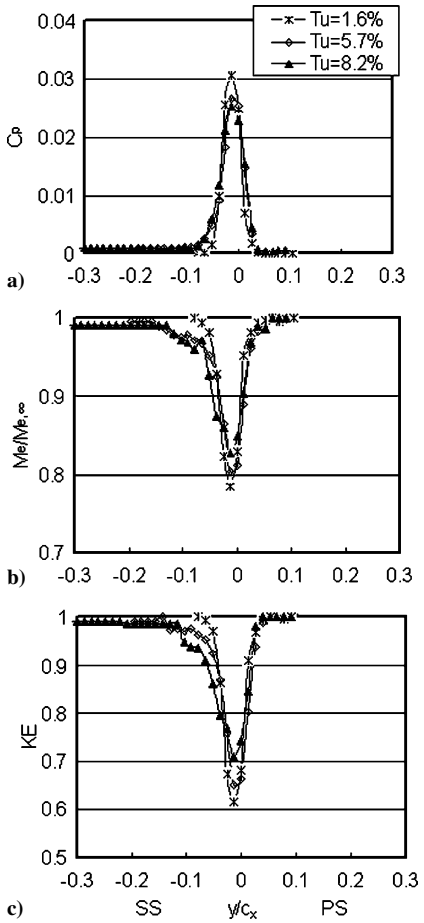

Fig. 4 Profiles measured at 0.25 axial chord lengths downstream of the test vane for $M_{ex} = 0.35$: a) normalized local total pressure losses, b) normalized local Mach numbers, and c) normalized local kinetic energy.

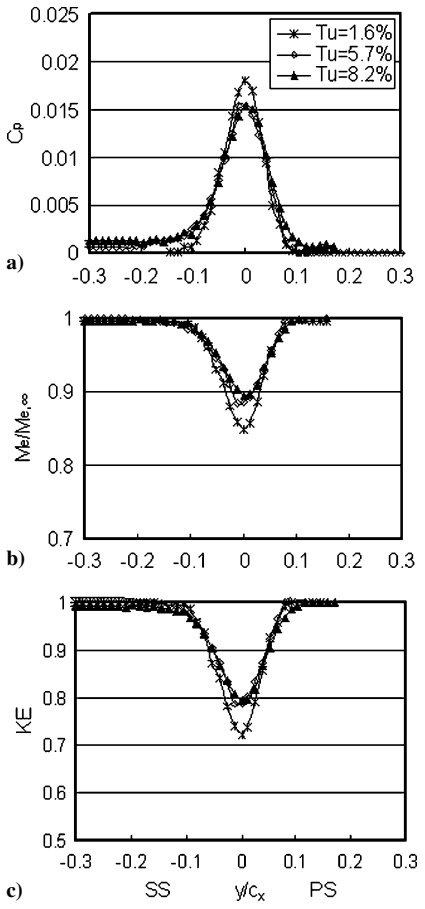

Fig. 5 Profiles measured at one axial chord length downstream of the test vane for $M_{ex} = 0.35$: a) normalized local total pressure losses, b) normalized local Mach numbers, and c) normalized local kinetic energy.

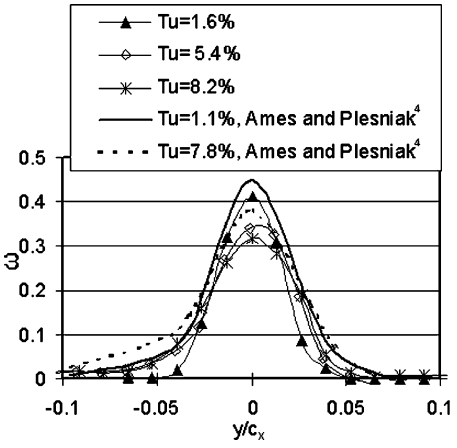

Fig. 6 Comparison of vane wake total pressure loss coefficient profiles measured 0.25 c_x downstream of a vane for $M_{ex} = 0.35$, with data from Ames and Plesniak[4] obtained 0.3c_x downstream of a vane for $M_{ex} = 0.27$.

addition, the growth and development of boundary layers on the suction and pressure sides are different. On the suction side, where local freestream velocities are higher, the boundary layers continue to become thicker up to the trailing edge. The thicker boundary layers then separate from the suction surface of the vane, which affects wake behavior immediately downstream of the trailing edge. On the pressure side, boundary-layer thickness is much smaller than that on the suction side as a result of locally higher flow acceleration. Bammert and Sandstede[17] report data showing that the boundary layer on the suction side is considerably thicker than on the pressure side. According to them, wake-profile losses are determined more by suction-side events by a factor about 2.5 to 3.5 times compared to events originating near the pressure side. Some other research groups find that differences in momentum losses between the suction surface and the pressure surface are even larger.

Figure 3 shows the effect of Mach number on normalized local total pressure losses C_p, normalized local Mach numbers $M_e/M_{e,\infty}$, and normalized local kinetic energy when no turbulence generator is installed. These data are measured in the wake at one chord length downstream of the trailing edge. Total pressure losses increase at each y/c_x location within the wake as the exit Mach number increases. The wake downstream of the vane also becomes wider at higher exit Mach numbers. This is a result of higher advection speeds, as well as increased diffusion within the wake. The change of the Mach-number distribution along the airfoil also affects the pressure gradient imposed on the boundary layer. In particular, the adverse pressure gradient present for $Bx/c_x > 0.80$ on the suction side of the $M_{ex} = 0.71$ vane is believed to induce local flow separation over this part of the vane surface. As a result, the C_p loss profile for $M_{ex} = 0.71$ is somewhat more substantial than profiles measured with $M_{ex} = 0.50$ and 0.35. Such changes are further verified by FLUENT predictions of C_p profiles, which are given in Fig. 3d and are also tied to increased sensitivity of flow behavior to vane geometry as the Mach number becomes higher. Also shown in Fig. 3 are normalized kinetic energy and Mach-number profiles, which appear to be less sensitive (than Cp profiles) to changes of the exit Mach number from $M_{ex} = 0.35$ to 0.50. Compressibility, which is important at the freestream Mach numbers investigated, produces alterations to the character and development of boundary layers, in addition to the other phenomena discussed.

Figures 4 and 5 present results that illustrate the effects of inlet turbulence intensity levels on normalized local total pressure losses

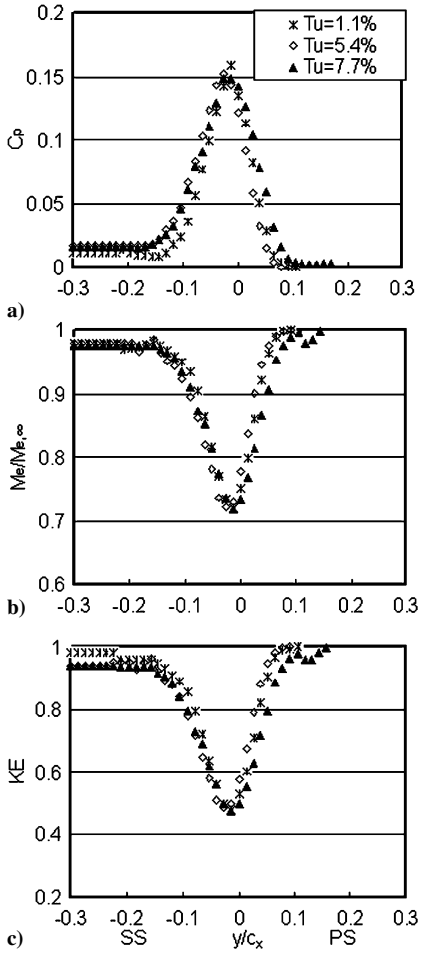

Fig. 7 Profiles measured at 0.25 axial chord lengths downstream of the test vane for $M_{ex} = 0.71$: a) normalized local total pressure losses, b) normalized local Mach numbers, and c) normalized local kinetic energy.

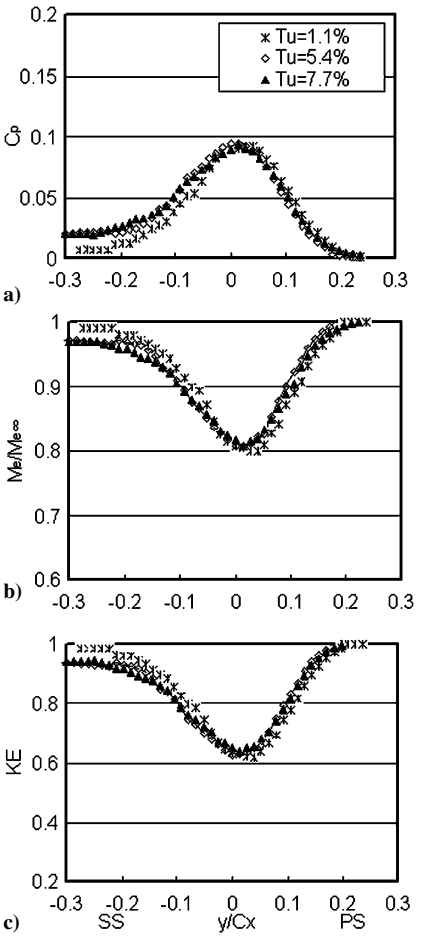

Fig. 8 Profiles measured at one axial chord length downstream of the test vane for $M_{ex} = 0.71$: a) normalized local total pressure losses, b) normalized local Mach numbers, and c) normalized local kinetic energy.

C_p, normalized local Mach numbers $M_e/M_{e,\infty}$, and normalized local kinetic energy profiles for $M_{ex} = 0.35$. The data in these two figures are measured in the wake at 0.25 axial chord lengths and one axial chord length downstream of the vane, respectively. Results are presented for Tu magnitudes of 1.6, 5.7, and 8.2%. As the inlet turbulence intensity increases, C_p values drop, and $M_e/M_{e,\infty}$ and KE values increase at the center of the wake at $y/c_x = 0$. The wake downstream of the airfoil also generally becomes wider, especially on the suction side, as the inlet turbulence intensity level increases. This is partially because the boundary layer on the suction surface is forced into transition earlier by the higher freestream turbulence level. Increased diffusion from the wake to surrounding freestream flow also plays an important role in producing such trends.

In their low-speed cascade experiments, Ames and Plesniak[4] also observe wake broadening with increasing mainstream turbulence intensity and associate these with smaller peak velocity deficits. These investigators define a total loss coefficient ω, which is given by

$$\omega = \frac{p_{oi} - p_{oe}}{p_{oi} - p_{se}} \tag{1}$$

The Ames and Plesniak[4] data are taken approximately 0.3 axial chord lengths downstream of a vane with $M_{ex} = 0.27$, compared to 0.25 axial chord lengths downstream of a vane with $M_{ex} = 0.35$ for the present study. The vane used by Ames and Plesniak[4] is two times the size of the vane from present study and has an exit angle of 72.4 deg, compared to an exit angle of 62.75 deg for the present investigation. Figure 6 shows that the two sets of data have similar trends and similar qualitative variations with Tu. In particular, both sets of data show decreasing ω magnitudes at $y/c_x = 0$ and broader wakes with higher ω magnitudes at negative y/c_x, as Tu becomes larger. The small quantitative differences are caused by slightly different vane configurations, flow conditions, and measurement locations relative to the vane trailing edges. Overall, the agreement between the two data sets not only provides verification of procedures and results from the present study, but also confirms the effects of inlet turbulence intensity level on vane aerodynamic losses in near-wake profiles for similar experimental conditions.

Note that wake profiles from the present study and from Ames and Plesniak[4] are both made over planes oriented approximately normal to the overall flow direction. In the case of Ames and Plesniak,[4] this is done by traversing the exit probe over curved arcs downstream of vanes. Note that freestream losses are present outside of the suction-side wakes (at negative y/c_x) in both investigations (the present study and Ames and Plesniak[4]) when inlet turbulence intensity levels are augmented. Such freestream losses are not observed by Zhang et al.[8] in their turbulence effect investigation where a symmetric airfoil is used with a zero angle of inclination, and the total pressure at inlet of test section is nearly the same as the value in the freestream at the outlet. This suggests that interactions between turbulence diffusion in a direction normal to the flow streamlines and inertial velocity gradients produce additional mixing losses near the cambered vanes.

Wake profiles for $M_{ex} = 0.71$ are shown in Figs. 7 and 8, which are measured at 0.25 axial chord lengths and one axial chord length downstream of the vane, respectively. At this higher exit Mach number (transonic flow), these wake profiles are less sensitive to changes of the inlet turbulence intensity level. Measurement data in Fig. 7 for various inlet turbulence intensity levels are qualitatively similar, except for changes caused by higher freestream losses outside

of the suction-side wakes (at negative y/c_x) at higher inlet turbulence intensity levels. Figure 8 also shows suction-side wake profiles (at negative y/c_x), which are widened appreciably from substantial freestream losses present at higher inlet turbulence intensity levels. When compared to results in Figs. 4 and 5, some differences are caused by compressibility and higher vane loading at the higher mainstream Mach numbers, which alter the development of boundary layers as well as the dependence of wake profiles on the inlet and mainstream turbulence intensity levels.

Integrated Aerodynamic Losses

Dimensional magnitudes of IAL are determined by integrating profiles of $(P_{oi} - P_{oe})$ with respect to y in the transverse flow direction across the wake for one single vane spacing, from $-p/2$ to $p/2$. In equation form, IAL is then given by

$$\mathrm{IAL} = \int_{-p/2}^{p/2} (p_{oi} - p_{oe})\,\mathrm{d}y \tag{2}$$

In present study, IAL magnitudes are mostly the result of two phenomena. These are 1) the losses resulting from formation of the boundary layers along the vane surfaces and 2) the flow separation, recirculation zone, and wake mixing losses that are initially present just downstream of the vanes. IAL magnitudes are determined from profiles that are measured 0.25 of one axial chord length and one axial chord length downstream of the turbine vane.

IAL data are normalized using the test-section passage pitch p and test-section inlet stagnation pressure P_{oi} in Fig. 9, which shows how IAL data vary with exit Mach number at the lowest inlet turbulence intensity level employed. IAL values increase as the exit Mach number increases, with dramatic increases in IAL magnitudes as the exit Mach number increases from 0.50 to 0.71. This is caused in part by the flow separation zone, which is present for $Bx/c_x > 0.80$ on the suction side of the $M_{ex} = 0.71$ vane. Therefore, development of suction-side boundary layers is different for this high Mach number than when $M_{ex} = 0.50$ and 0.35. Compressibility also plays some role in this substantial change. Such behavior is also consistent with experimental and analytical results by Joe et al.[10] and Xu and Denton,[18] who show that total pressure losses increase approximately with the square of the Mach number.

Symmetric airfoil results from Zhang and Ligrani[9] are also included in Fig. 9. Similar qualitative trends are observed between these two studies, however, when compared at the same exit Mach number, the present normalized IAL data for cambered test vanes are much higher than data obtained downstream of straight symmetric airfoils without flow turning. This is caused by different flow development over the symmetric and cambered airfoils from different pressure gradients and different amounts of streamline curvature, which are imposed on airfoil boundary layers. Such imposed pressure gradients are a result of airfoil shape, the imposed Mach-number distribution, and streamline curvature and flow turning in the flow outside of the boundary layers.

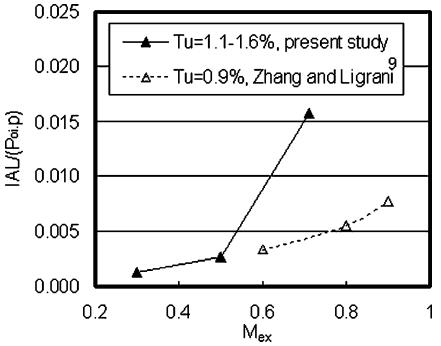

Fig. 9 Comparison of normalized integrated aerodynamic loss magnitudes as dependent upon exit Mach number and measured one chord length downstream of the airfoils.

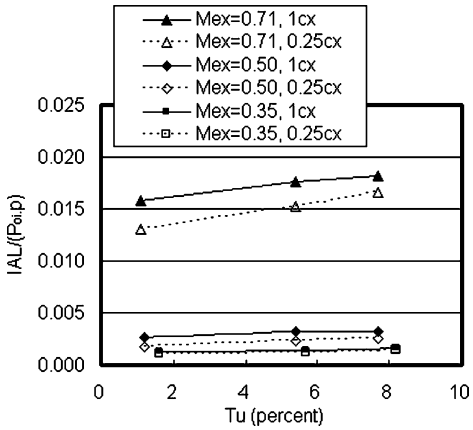

Fig. 10 Comparison of normalized integrated aerodynamic losses as dependent upon inlet turbulence intensity.

Normalized IAL data are presented in Fig. 10 as dependent upon the inlet turbulence intensity level for three exit Mach numbers, as measured 0.25 of one axial chord length and one axial chord length downstream of the turbine vane. For each exit Mach number and each measurement location, the normalized IAL data in this figure increase slightly as the inlet turbulence intensity level increases. The IAL differences at each M_{ex} for the $1c_x$ and $0.25c_x$ downstream measurement locations are relatively small compared to overall IAL loss magnitudes. This is a result of how momentum and turbulence kinetic energy are budgeted and conserved through the wake. Near the vane trailing edge, most turbulence in the wake is initially produced in the separated and recirculating flow zones, which give the initial condition for wake-profile development, as well as initial values of turbulence at beginning of the wake. As the wake continues to develop downstream, turbulence decays with streamwise distance because turbulence production is less than diffusion and advection. As a result, the shape of momentum deficit changes mostly because of the transverse diffusion of momentum. Overall magnitudes of total pressure deficits and momentum deficits then do not change greatly as the wake is advected in the streamwise direction because not much mean streamwise momentum is converted into turbulence by local shear and turbulence production. Such trends in the present data are consistent with results presented by Mee et al.,[19] who suggest that most entropy increases take places close to the trailing edge of the airfoils. Additional mixing losses are then only a small fraction of overall loss magnitudes.

Area-Averaged Loss Coefficients

Different loss coefficient definitions are sometimes employed by different research groups. Of these, Boyle and Senyiko[20] and Boyle et al.[3] employ an area-averaged loss coefficient Y_A in their analysis, which is defined using an equation of the form

$$Y_A = \frac{p_{oi} - p_{oe,A}}{p_{oi} - p_{se,A}} \tag{3}$$

These are determined using equations respectively given by

$$p_{oe,A} = \int_{-p/2}^{p/2} p_{oe}\,\mathrm{d}\left(\frac{y}{p}\right) \tag{4}$$

and

$$p_{se,A} = \int_{-p/2}^{p/2} p_{se}\,\mathrm{d}\left(\frac{y}{p}\right) \tag{5}$$

Boyle and Senyiko[20] employ vanes with 5.18-cm axial chord length and 75-deg flow turning angle. Boyle et al.[3] employ vanes with 4.445-cm axial chord length and approximately 80-deg flow turning angle in their numerical prediction. Their data are based on measurements made in axial plane located 0.29 axial chord length downstream of their vane trailing edge. Figure 11 shows comparisons of

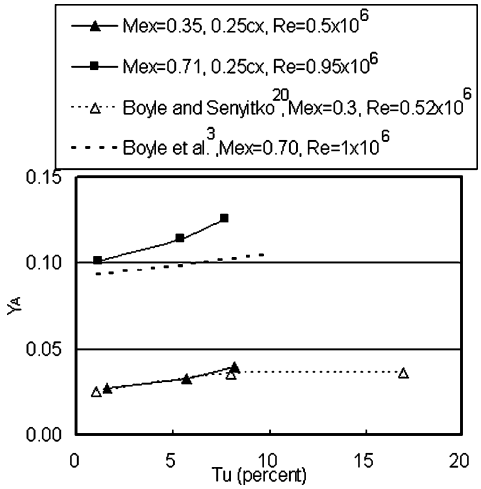

Fig. 11 Comparison of area-averaged loss coefficients measured in normal planes $0.25c_x$ downstream of the vane, with values from Boyle and Senyitko[20] and Boyle et al.[3] obtained in axial planes located $0.35c_x$ downstream of their airfoils.

their data with results from the present study over a range of exit Mach numbers, which are measured in normal planes $0.25c_x$ downstream of the vane. These data indicate that higher Y_A losses are generally observed as higher inlet turbulence intensity levels are present. Excellent agreement is shown in Fig. 11 between results from Boyle and Senyiko[20] and the present study at relatively low exit Mach number. For the present study, $M_{ex} = 0.35$ and $Re = 0.5 \times 10^6$, whereas $M_{ex} = 0.3$ and approximately $Re = 0.52 \times 10^6$ for Boyle and Senyiko.[20] Predicted values at high exit Mach numbers are slightly lower than the present experimental results, but differences are relatively small, and trends are generally consistent. Here, $M_{ex} = 0.7$ and $Re = 1 \times 10^6$ for Boyle et al.[3] compared to $M_{ex} = 0.71$ and $Re = 0.95 \times 10^6$ for the present study. Therefore, to some extent, the present experimental data validate the numerical code and procedures employed by Boyle et al.[3]. Note that some differences between the present results and those from Boyle et al.[3] and Boyle and Senyiko[20] are caused by different wake traversing procedures. Whereas profiles from the present study are measured in planes that are oriented normal to the backflow direction, wake data from the other investigations[3,20] are given for axial planes.

Summary

The effects of inlet turbulence intensity and exit Mach number on the aerodynamic performance of a turbine vane (which models a vane from an operating gas turbine engine) are investigated. Three different Mach-number distributions are employed, which result in one transonic flow and two subsonic flows. All three Mach-number distributions match distributions from different operating engine environments. A fine-mesh grid and cross bars are used to augment the magnitudes of longitudinal turbulence intensity at the inlet of the test section, so that a total of three different inlet turbulence intensity levels is employed. Wake-profile data are presented for two different locations downstream of the vane trailing edge.

Wake profiles of total pressure losses, Mach-number deficits, and deficits of kinetic energy are asymmetric. This is because of different loading, different boundary-layer growth, and different susceptibility to flow separation on the different vane surfaces, which also causes the suction side wakes (at negative y/c_x) to be thicker than the pressure side wakes (at positive y/c_x). The wake downstream of the vane becomes wider at higher exit Mach numbers as a result of higher advection speeds, as well as increased diffusion within the wake. Particularly, the loss profile for $M_{ex} = 0.71$ is somewhat more substantial than profiles measured with $M_{ex} = 0.50$ and 0.35. This is partially because of local flow separation caused by the adverse pressure gradient present for $Bx/c_x > 0.80$ on the suction side of the $M_{ex} = 0.71$ vane.

Wake profiles also become broader with increased turbulence intensity levels, especially on the suction side. This is partially caused by suction-side boundary layers, which are forced into transition farther upstream by the higher magnitudes of freestream turbulence. Increased diffusion from the wake to surrounding freestream flow also plays a role in producing such trends. In general, wake profiles are more sensitive to changes and augmentations of turbulence intensity at lower subsonic flow conditions than when transonic flow is present.

Integrated aerodynamic loss (IAL) magnitudes increase as higher Mach numbers are present along the airfoil. When compared at the same exit Mach number, the present normalized IAL data for cambered test vanes are much higher than data obtained downstream of straight symmetric airfoils without flow turning. Overall, this means that greater losses are present with flow turning and cambered airfoils, than with symmetric airfoils. Magnitudes of IAL also slightly increase as the inlet turbulence intensity level increases. The IAL differences obtained for each vane Mach-number distribution for the $1c_x$ and $0.25c_x$ downstream measurement locations are relatively small compared to overall IAL loss magnitudes. This is because not much mean streamwise momentum is converted into turbulence by local shear and turbulence production as the wake is advected in the streamwise direction.

Higher magnitudes of area-averaged loss coefficients Y_A are also generally observed in this study as either higher inlet turbulence intensity levels or higher exit Mach numbers are present. Excellent agreement is present between results from Boyle and Senyiko[20] and the present study for a low subsonic Mach-number distribution along the vane, which gives an exit Mach number M_{ex} of 0.35. Other experimental data from the present investigation show similar qualitative trends and validate the numerical predictions by Boyle et al.[3] for a similar vane configuration when the Mach-number distribution along the vane is transonic and $M_{ex} = 0.71$.

Acknowledgments

The research reported in this paper was sponsored by the National Science Foundation (NSF Grant Number CTS-0086011). Stefan Thynell and Richard Smith were the NSF program monitors. The authors also acknowledge Mike Blair of Pratt and Whitney Corporation; Hee-Koo Moon of Solar Turbines, Inc.; Edward North and Ihor Diakunchak of Siemens–Westinghouse Corporation; and Sri Sreekanth and Ricardo Trindade from Pratt and Whitney–Canada Corporation for guidance and suggestions on this research effort.

References

[1]Geogory-Smith, D. G., and Cleak, J. G. E., "Secondary Flow Measurements in a Turbine Cascade with High Inlet Turbulence," *Journal of Turbomachinery*, Vol. 114, Jan. 1992, pp. 173–183.

[2]Giel, P. W., Bunker, R. S., Van Fossen, G. J., and Boyle, R. J., "Heat Transfer Measurements and Predictions on a Power Generation Gas Turbine Blade," American Society of Mechanical Engineers, Paper 2000-GT-209, 2000.

[3]Boyle, R. J., Luci, B. L., Verhoff, V. G., Camperchioli, W. P., and La, H., "Aerodynamics of a Transitioning Turbine Stator over a Range of Reynolds Numbers," American Society of Mechanical Engineers, Paper 98-GT-285, 1998.

[4]Ames, F. E., and Plesniak, M. W., "The Influence of Large-Scale, High Intensity Turbulence on Vane Aerodynamics Losses, Wake Growth, and the Exit Turbulence Parameters," *Journal of Turbomachinery*, Vol. 119, April 1997, pp. 182–192.

[5]Jouini, D. B. M., Sjolander, S. A., and Moustapha, S. H., "Aerodynamic Performance of a Transonic Turbine Cascade at Off-Design Conditions," *Journal of Turbomachinery*, Vol. 123, July 2001, pp. 510–518.

[6]Radomsky, R. W., and Thole, K. A., "Detailed Boundary Layer Measurements on a Turbine Stator Vane at Elevated Freestream Turbulence Levels," *Journal of Turbomachinery*, Vol. 124, Jan. 2002, pp. 107–118.

[7]Boyle, R. J., Lucci, B. L., and Senyitko, R. G., "Aerodynamics Performance and Turbulence Measurements in a Turbine Vane Cascade," American Society of Mechanical Engineers, Paper GT-2002-30434, 2002.

[8]Zhang, Q., Lee, S. W., and Ligrani, P. M., "Effects of Surface Roughness and Turbulence Intensity on the Aerodynamic Losses Produced by the Suction Surface of a Simulated Turbine Airfoil," *Journal of Fluids Engineering*, Vol. 126, March 2004, pp. 257–265.

[9]Zhang, Q., and Ligrani, P. M., "Effects of Mach Number and Surface Roughness on the Aerodynamic Losses of a Symmetric Transonic Turbine Airfoil," *Journal of Propulsion and Power*, Vol. 20, No. 6, 2004, pp. 1117–1125.

[10]Joe, C. R., Montesdeoca, X. A., Soechting, F. O., MacArthur, C. D., and Meininger, M., "High Pressure Turbine Vane Annular Cascade Heat Flux and Aerodynamic Measurements with Comparisons to Predictions," American Society of Mechanical Engineers, Paper 98-GT-430, 1998.

[11]Coton, T., Arts, T., and Lefebvre, M., "Effects of Reynolds and Mach Numbers on the Profile Losses of a Conventional Low-Pressure Turbine Rotor Cascade with an Increasing Pitch-Chord Ratio," *Proceedings of the Institution of Mechanical Engineers, Part A: Journal of Power and Energy*, Vol. 215, No. 6, 2001, pp. 763–772.

[12]Jackson, D. J., Lee, K. L., Ligrani, P. M., and Johnson, P. D., "Transonic Aerodynamics Losses due to Turbine Airfoil, Suction Surface Film Cooling," *Journal of Turbomachinery*, Vol. 122, April 2000, pp. 317–326.

[13]Furukawa, T., and Ligrani, P. M., "Transonic Film Cooling Effectiveness from Shaped Holes on a Simulated Turbine Airfoil," *Journal of Thermophysics and Heat Transfer*, Vol. 16, April–June 2002, pp. 228–237.

[14]Kline, S. J., and McClintock, F. A., "Describing Uncertainties in Single Sample Experiments," *Mechanical Engineering*, Vol. 75, 1953, pp. 3–8.

[15]Moffat, R. J., "Describing the Uncertainties in Experimental Results," *Experimental Thermal and Fluid Science*, Vol. 1, 1988, pp. 3–17.

[16]Jackson, D. J., "Aerodynamic Mixing Losses and Discharge Coefficients due to Film Cooling From a Symmetric Turbine Airfoil in Transonic Flow," M.S. Thesis, Dept. of Mechanical Engineering, Univ. of Utah, Salt Lake City, Aug. 1998.

[17]Bammert, K., and Sandstede, H., "Measurements of the Boundary Layer Development Along a Turbine Blade with Rough Surfaces," *Journal of Engineering for Power*, Vol. 102, Oct. 1980, pp. 978–983.

[18]Xu, L., and Denton, J. D., "The Base Pressure and Loss of a Family of Four Turbine Blades," *Journal of Turbomachinery*, Vol. 10, Jan. 1988, pp. 9–17.

[19]Mee, D. J., Braines, N. C., Oldfield, M. L. G., and Dickens, T. E., "An Examination of the Contributions to Loss on a Transonic Turbine Blade in Cascade," *Journal of Turbomachinery*, Vol. 114, Jan. 1992, pp. 155–162.

[20]Boyle, R. J., and Senyitko, R. G., "Measurements and Predictions of Surface Roughness Effects on Turbine Vane Aerodynamics," *Proceedings of ASME Turbo Expo 2003*, Paper GT 2003-38580, June 2003.